THE JOURNAL OF PHYSICAL CHEMISTRY C

Article

Evidence for Considerable Metal Cation Concentrations from Lithium Intercalation Compounds in the Nano-Bio Interface Gap

Merve Dogangun, Mimi N. Hang, Jo Machesky, Alicia C. McGeachy, Naomi Dalchand, Robert J Hamers, and Franz M. Geiger

J. Phys. Chem. C, **Just Accepted Manuscript** • DOI: 10.1021/acs.jpcc.7b09187 • Publication Date (Web): 10 Nov 2017

Just Accepted

ACS Publications

The Journal of Physical Chemistry C is published by the American Chemical Society. 1155 Sixteenth Street N.W., Washington, DC 20036

Evidence for Considerable Metal Cation Concentrations from Lithium Intercalation Compounds in the Nano-Bio Interface Gap

Merve Doğangün,[1] Mimi N. Hang,[2] Jo Machesky[1], Alicia C. McGeachy,[1] Naomi Dalchand,[1] Robert J. Hamers,[2] Franz M. Geiger[1]

[1]Department of Chemistry, Northwestern University, Evanston, IL 60208, United States,

[2]Department of Chemistry, University of Wisconsin, 1101 University Avenue, Madison, WI, 53706, United States

ABSTRACT. An experimental investigation of how electrostatics and ion dissolution impact the interaction between nanosheets of lithium intercalation compounds and supported lipid bilayers has revealed evidence for considerable metal cation concentrations in the nanosheets/bilayer (the "nano-bio interface") gap. Specifically, elevated concentrations of aqueous metal ions in the 1 mg/L concentration regime produce vibrational sum frequency generation signal intensity changes that are commensurate with the induction of compositional membrane asymmetry. This outcome is consistent with the notion that the induction of bilayer asymmetry by $LiCoO_2$ nanosheets occurs through a non-contact mechanism that involves primarily the interaction of negatively charged lipids with dissolved ions concentrated within the electrical double layers present in the nano-bio interface gap. Our findings provide opportunities for mitigating non-contact interactions between nanomaterials and biological interfaces and point towards a path for enabling the design of new energy storage materials with reduced environmental impacts.

*Corresponding Author. Email: geigerf@chem.northwestern.edu.

I. INTRODUCTION. The increasing use of nanoscale redox-active materials in all-electric/hybrid vehicles and grid energy storage, specifically lithium intercalation compounds,[1-3] may lead to environmental release and exposure,[4-5] with poorly understood biological outcomes.[6-8] Recent studies have explored metal oxide nanoparticle toxicity to prokaryotic and eukaryotic cells, as well as unicellular and multicellular organisms.[9-12] Some of the commonly proposed mechanisms of cytotoxicity include the generation of reactive oxygen species, release of metal ions, penetration of the cell envelope, and the disorganization of bacterial membrane.[13-17] As the toxicity mechanisms of metal oxide nanomaterials may vary fundamentally depending on the properties of nanomaterials as well as the membrane structures, a detailed molecular-level understanding of how redox active nanomaterials interact with cell membranes or model cell membranes, including supported phospholipid bilayers (SLBs), warrants exploration.

We have previously shown that lithium cobalt oxide ($LiCoO_2$) nanosheets induce alterations to the compositional asymmetry in two-component SLBs through electrostatic interactions.[18] Here, we further explore the charge interactions by altering the ζ-potential of nanosheets and changing the ionic strength of the solution. Yet, while many nanomaterials are poorly soluble in water, dissolution of some metal oxide nanoparticles, including those containing TiO_2, ZnO, and CuO, in aqueous environments may result in cellular toxicity due to the release of Ti^{2+}, Zn^{2+}, and Cu^{2+} ions into solution.[19-20] Indeed, previous work by Hang *et al.* demonstrated that the toxicity of nanoscale lithium nickel manganese cobalt oxide (NMC) to the Gram-negative bacterium *Shewanella oneidensis* MR-1 arises from the incongruent release of transition metal ions (specifically Ni^{2+} and Co^{2+}) into solution, as opposed to the nanoparticles themselves.[16] Specifically, that study showed that Co^{2+} significantly delayed the onset of exponential growth at sub mg/L concentrations, while Li^+ had no effect on bacterial growth.[16] For simultaneous exposure to both Li^+ and Co^{2+}, total oxygen

consumption remained unchanged. Subsequent research investigated the impact of chemical composition of NMC on bacterial oxygen consumption,[17] and how the surface structure of $LiCoO_2$ nanosheets can be altered to enhance phosphate binding,[21] so as to decrease ion dissolution by an environmentally acquired surface coating. In this present work, we aim to address the possible importance of ion dissolution from the $LiCoO_2$ nanosheets for the induction of compositional asymmetry in supported lipid bilayers. To this end, we present results from vibrational sum frequency generation (SFG) spectroscopy experiments sensitive to how the chemical composition of SLBs may or may not change upon exposure to aqueous Li^+ and Co^{2+} ions. SFG spectroscopy has previously been used to probe the kinetics of transbilayer movement of lipids and bilayer asymmetry at aqueous/solid interfaces,[22-25] as well as to obtain structural and orientational information on aqueous ion-phospholipid interactions at the air/water interface.[26-27] Our studies provide empirical evidence for a locally high concentration of ions present at the bilayer-nanosheet gap, and provide estimates for the dissolved ion concentrations at the interfacial region, which may ultimately be helpful for to abating potential environmental impacts of nanomaterials used for energy storage.

II. EXPERIMENTAL.

A. Bilayer Preparation. 1,2-dimyristoyl-*sn*-glycero-3-phosphocholine (DMPC) and 1,2-dimyristoyl-*sn*-glycero3-phospho-(1-*rac*-glycerol) (DMPG) were purchased from Avanti Polar Lipids and used without further purification. Lipid bilayers from small unilamellar vesicles of pure DMPC as well as a lipid mixture containing 90 mol% DMPC and 10 mol% DMPG were prepared on 3mm thick IR-grade fused silica windows (ISP Optics) by the vesicle fusion method, as described earlier.[18, 28-29] Experiments were carried out at room temperature (22 ± 1 ^oC). All SLBs were formed at 0.01 M Tris or 0.01 M HEPES buffer and 0.1 M NaCl in the presence of 0.005 M $CaCl_2{\cdot}2H_2O$ at pH 7.40 ± 0.03, and rinsed with Ca-free buffer following bilayer formation.

B. Dynamic Light Scattering (DLS) of Nanosheets. Diffusion coefficients, electrophoretic mobilities, *z-A*verage hydrodynamic diameters (nm) and apparent ζ-potentials for fresh suspensions (5 mg/L) of $LiCoO_2$ nanosheets and vesicle solutions were determined using a Malvern Instruments Zetasizer Nano, with a He-Ne laser at 633 nm operating at a maximum of 5 mW. Electrophoretic mobility was converted to ζ-potential by the Smoluchowski model which simply assumes spherical particles.[30] We note that nanosheets have different aspect ratios that might lead to deviations in the absolute values. $LiCoO_2$ nanosheet suspensions were sonicated in 0.1 M NaCl, 0.01 M Tris or HEPES buffer at pH 7.4 for 10 minutes and vortexed for 30 seconds.

C. Nanosheet Imaging on Supported Lipid Bilayers. A Leo Supra55 VP scanning electron microscope (SEM) coupled with a Thermo Scientific UltraDry energy-dispersive X-ray spectroscopy (EDS) detector was used to probe for the presence of attached $LiCoO_2$ nanosheets on SLBs formed from unilamellar vesicles prepared from a 9:1 mix of DMPC/DMPG in Tris buffer on 5% thermal oxide ultraflat SiO_2 wafers.[18] In HEPES buffer, the nanosheet attachment to SLBs was probed by SEM (Hitachi SU8040) coupled with an Oxford Aztec X-max 80 EDS detector. The images were taken using 14 keV incident electron energy.

D. Metal Ion Dissolution from $LiCoO_2$ Nanosheets. A PerkinElmer Optima 2000 inductively couple plasma (ICP) optical emission spectrometer (OES) was used to determine metal concentrations of the $LiCoO_2$ nanosheets in aqueous solutions held at 0.1M NaCl, 0.01M Tris and pH 7.4. To characterize metal ion release into the solution, triplicate sample suspensions of $LiCoO_2$ at 5 mg/L concentration was prepared. After 4 hours, the suspensions were centrifuged at 4,700g for 10 minutes to remove most of the $LiCoO_2$ nanoparticles in solution. The supernatants were then ultracentrifuged for 2 hours at 288,000g using a Beckman Coulter Optima Ultracentrifuge with a SW-41 Ti Rotor to ensure removal of any

remaining $LiCoO_2$ nanoparticles. Concentrations of dissolved metal species in the resulting supernatants were measured by ICP-OES. Stock solutions of LiCl and $CoCl_2.6H_2O$ in 0.01 M Tris buffer and 0.1 M NaCl at pH 7.4 at metal ion concentrations equivalent to those measured by ICP-OES were used as described in the Results section.

E. Vibrational Sum Frequency Generation Spectroscopy. Details of our SFG approach and experimental setup for probing condensed matter interfaces have been reported previously.[18, 31-33] Experimental details regarding the solution preparation, bilayer formation and characterization, and flow conditions have been reported recently as well.[18, 29] Briefly, we followed the SFG signal intensity attributed to the terminal CH_3-ν_s (symmetric stretch) in the lipids used in our bilayers to evaluate changes in SLB asymmetry upon exposure to the oxide nanosheets or the dissolved metal ions. We selectively probed vibrational modes having transition dipole moment orientation components perpendicular to the liquid/solid interface. The SFG spectra were recorded in triplicate for each experimental condition of varying buffer identity, oxide nanosheet, bare ion identity, bare ion concentration and ionic strength.

F. Second Harmonic Generation $\chi^{(3)}$ Spectroscopy. The SHG studies reported here were carried out using the methods described previously,[29, 31] using the s-in/all out polarization combination.

III. RESULTS AND DISCUSSION.

A. $LiCoO_2$ Nanosheet Interactions with SLBs Formed from 9:1 Mixtures of DMPC/DMPG Lipids Depend Critically on ζ-Potential at 0.1 M NaCl. We first examined the effect of buffer choice and ζ-potential on nanosheet-bilayer interactions (Table I). While $LiCoO_2$ nanosheets suspended in 0.1M NaCl, 0.01 M Tris buffer exhibit positive ζ-potentials (+12.9 ± 0.6 mV),[18] they were found to exhibit negative ζ-potentials (−19.4 ± 1.8 mV) when suspended in solutions prepared using 0.1M NaCl and 0.01 M HEPES buffer. This difference in ζ-potentials for the two different buffers is putatively attributed to the possibly surface-

active nature of the Tris cation, which has been previously reported to be present at silica and bilayer surfaces.[18, 29] This finding also highlights the importance of buffer choice when studying oxide nanosheets at the nano-bio interface. Note that while the ζ-potentials of nanosheet suspensions show differences in the two different buffers, the ζ-potentials of the vesicles formed from the 9:1 mixture of DMPC/DMPG lipids used for preparing the supported lipid bilayers studied in this work remain invariant in the two buffers. The complete characterization data are provided in the Supporting Information Table S1.

We used SEM/EDS to provide evidence of $LiCoO_2$ nanosheet attachment to bilayers formed from the 9:1 mixture of DMPC/DMPG used in these experiments.[18] Figure 1A shows the SEM image and the corresponding EDS spectra of an ultraflat SiO_2 wafer with a bilayer prepared from a 9:1 mixture of DMPC/DMPG lipids in 0.1 M NaCl buffered at pH 7.4 using 0.01 M Tris buffer. Following nanosheet exposure and rinse, the EDS data reveals localized regions of the bilayer contained $LiCoO_2$ nanosheets, identified at 0.79 and 7.65 keV for cobalt, that are readily distinguished from Na (1.04 keV) and Cl (2.62 keV) signals originating from the cubic feature seen in the image and Si (1.74 keV) and O (0.52 keV) signals from the underlying SiO_2 substrate.

Switching from Tris to HEPES buffer would be expected to lead to some degree of Coulombic repulsion between the negatively charged bilayers and the $LiCoO_2$ nanosheets, which carry a negative potential in HEPES buffer.[29] Indeed, as shown in Figure 1B, the flake-like $LiCoO_2$ structures in HEPES buffer are present but in more confined regions compared to Tris. EDS data shows the presence of $LiCoO_2$ nanosheets in localized regions, identified at 0.78, 6.92 and 7.65 keV for cobalt. Signals originating from the cubic feature seen in the image are from Na (1.04 keV) and Cl (2.62 and 2.82 keV) and signals from the underlying SiO_2 substrate appear at 1.74 keV for Si and at 0.52 keV for O.

To probe the nanosheet-bilayer interactions *in situ*, and under conditions of dynamically changing aqueous flow, we proceeded to record vibrational SFG spectra of the supported lipid bilayers before, during, and after exposure to the oxide nanosheets. Figures 2A and 2B show representative SFG spectra of 9:1 DMPC/DMPG bilayers maintained in 0.01 M Tris and in 0.01 M HEPES buffer, respectively, both in the presence of 0.1 M NaCl at pH 7.4. Before the addition of the $LiCoO_2$ nanosheets, the SLBs produce vibrational SFG spectra featuring comparable peak positions at *ca.* 2980, 2930, and 2880 cm^{-1}, where the 2880 cm^{-1} peak which is attributed to the CH_3 symmetric stretch of the alkyl tails and the other two features are presumably due to interference from the O−H stretches.[18, 34-36] We note that the relative signal intensities vary somewhat with choice of buffer. Unlike the previously examined $LiCoO_2$ nanosheets suspended in Tris buffer, which show SFG signal increases that are attributable to asymmetry induction in the membrane (Fig. 2A),[18] the SFG responses from the bilayer remain invariant upon exposing it to $LiCoO_2$ nanosheets suspended in 0.01M HEPES buffer (Fig. 2B). A similar lack of a signal intensity change was observed when NMC nanosheets, carrying a negative ζ-potential of -19.5 ± 1.4 mV in 0.01 M Tris buffer and 0.1 M NaCl were exposed to bilayers formed from 9:1 mixture of DMPC/DMPG at 0.1 M NaCl.[18] These two results suggest that negatively charged nanosheets do not induce compositional asymmetry in supported lipid bilayers formed from 9:1 mixtures of DMPC/DMPG under the solution conditions used in our experiments, a likely result of Coulombic repulsion, given that the bilayers studied here carry a negative surface potential under the conditions of our experiments.[29]

B. $LiCoO_2$ Nanosheets Do Not Disturb SLBs Formed from 9:1 Mixtures of DMPC/DMPG Lipids at Low Ionic Strength. To investigate the role of ionic strength on the oxide nanosheet-bilayer interactions, we rinsed bilayers formed in 0.1 M NaCl and 0.01 M Tris buffer with a solution of 0.001 M NaCl in 0.01 M Tris buffer and subsequently

exposed them at that low ionic strength to $LiCoO_2$ nanosheets maintained in Tris buffer. Fig. 2C shows that while the general lineshape of the SFG spectra obtained at high vs. low ionic strength in the presence of 0.01 M Tris buffer is invariant with salt concentration, the signal intensities tend to be higher at low salt concentration than at high salt concentration. Fig. 2D shows that exposing the SLBs to $LiCoO_2$ nanosheets suspended in 0.001 M NaCl and 0.01 M Tris buffer at pH 7.4, conditions for which the nanosheet ζ-potential is −9.4 ± 0.8 mV (Table I), leads only to insignificant SFG signal intensity changes. This outcome is attributable to the notion that despite reduced charge screening at low ionic strength, considerable charge-charge repulsion remains such that the oxide nanosheets cannot readily approach the bilayer to induce chemical asymmetry, as probed by SFG spectroscopy.

C. Dissolution of $LiCoO_2$ Nanosheets in Aqueous Solution Releases Li^+ and Co^{2+} Ions. Having established that $LiCoO_2$ nanosheets that carry a positive ζ-potential produce SFG signal intensity increases that indicate the induction of chemical asymmetry within supported lipid bilayers formed from 9:1 mixtures of DMPC/DMPG at 0.1 M NaCl, while those carrying a negative ζ-potential do not (even though they are still present at the bilayer, as evidenced by SEM), we proceeded to further investigate the fundamental interactions that lead to chemical asymmetry in bilayers exposed to oxide nanosheets. Our prior work[18] established that bilayers prepared from purely zwitterionic lipids do not produce SFG signal intensity changes upon exposure to $LiCoO_2$ nanosheets under conditions of 0.1 M salt and 0.01 M Tris buffer, while those prepared from mixes containing 10 mol% of the negatively charged lipids PS or PG do. This finding pointed to the importance of the lipids with negatively charged headgroups in the bilayer. Motivated by the extent of oxide dissolution reported for nanoscale lithium nickel manganese cobalt oxide by Hang *et al.*,[16] we asked whether the $LiCoO_2$ nanosheets studied in this present work could release metal cations directly into the membrane-nanosheet gap, where those metal cations (as opposed to the

actual nanosheets) could interact with the lipids to produce the observed SFG signal intensity changes described here.

Incongruent oxide dissolution may release metal cations in amounts that depend on the intrinsic properties of the oxide (*e.g.*, chemical composition and particle size) as well as the aqueous solution conditions (*e.g.*, pH, temperature, ionic strength).[37] Under the conditions of our experiment (0.1 M salt, 0.01 M Tris buffer, pH 7.4, and room temperature), our ICP-OES measurements (Table II) show, for suspensions of 5 mg/L $LiCoO_2$ stirred for four hours, dissolved Li ions at 0.124 ± 0.002 mg/L and dissolved Co ions at 0.042 ± 0.001 mg/L. Table II also shows that the extent of dissolution is fairly comparable for conditions of 0.001 M salt and 0.01 M Tris buffer. Ion dissolution for the condition of using HEPES buffer is comparable to that of Tris buffer.

Given the above findings, any experiment testing whether the presence of dissolved ions from the $LiCoO_2$ nanosheets cause the observed SFG signal intensity increases produced by the bilayers upon exposure to the nanosheets should then start with sub-mg/L concentrations of Li and Co ions dissolved in 0.1 M salt solution maintained at pH 7.4 using 0.01 M Tris buffer. Controls for chloride and any minor changes in ionic strength would be provided by adding sub-mg/L amounts of NaCl to the 0.1 M salt solution while monitoring the SFG spectra obtained from the bilayers. The following two sections present the results from those experiments.

D. Sub-mg/L Concentration of Aqueous Metal Ions Found in Bulk Nanosheet Solution Do Not Induce Apparent Bilayer Asymmetry from Bilayers Formed from 9:1 Mixture of DMPC/DMPG. As shown in Figure 3A and 3B, the presence of Li^+ and Co^{2+} ions at concentrations determined by ICP-OES to be relevant for $LiCoO_2$ nanosheet dissolution in high ionic strength does not produce significant SFG signal intensity increases in the spectra obtained from the bilayers. We further investigated possible combined ion effects by

introducing a solution containing both Li^+ and Co^{2+} ions using the concentrations determined in the dissolution experiments. Figure 3C shows negligible changes in the SFG spectra upon exposing bilayers to aqueous solutions under those conditions as well. Controls shown in Figure 3D indicate no change in the spectral lineshape when adding even one mg/L NaCl to the aqueous solution.

E. Elevated Concentrations of Aqueous Metal Ions Elicit Increases in SFG Signal Intensity from 9:1 DMPC/DMPG Bilayers. Although ICP-OES measurements yield information about dissolved ion concentration in the solution phase, these concentrations do not necessarily correlate to the effective concentration of ions at the bilayer/nanosheet interface. We therefore exposed bilayers prepared from a 9:1 mixture of DMPC/DMPG to Li^+ and Co^{2+} ion concentrations 10 times above those determined in the nanosheet dissolution studies, at a total salt concentration of 0.1 M and at pH 7.4, maintained using 0.01 M Tris buffer. As shown in Figures 4A and 4B, the use of elevated ion concentrations indeed produced significant SFG signal intensity increases for the case of Li^+ and Co^{2+} ions. Again, these results are for solution conditions of 0.01 M Tris buffer and 0.1 M NaCl. As shown in in the Supporting Information Figure S1, this result is robust over three measurements. Given the salt control (shown in Figure 3D), this outcome appears to point towards a role of ion specificity. The interaction appears to involve the negatively charged PG headgroup, as the introduction of 0.5 mg/L solution of Co^{2+} shown in Figure 4C respectively does not significantly alter the SFG signal intensity from bilayers composed of purely zwitterionic DMPC lipids, as shown in Figure 4C. Furthermore, Figure 4D shows that the increases in SFG signal intensity upon exposure to 0.5 mg/L Co^{2+} persist even upon rinsing.

Cation bonding to the backbone of peptides has been reported to depend on the hydration shell of the cation, with well-hydrated divalent cations showing stronger binding than weakly hydrated monovalent cations.[38] Similarly, the tendency of ions to interact with lipids in the

bilayer membrane depends on the strength of their hydration shell,[39-40] with anionic lipids typically more prone to strong interactions with metal cations than zwitterionic lipids because of attractive Coulombic forces.[41] McLaughlin and coworkers showed that Co^{2+} forms strong complexes with phoshatidylglycerol (PG) and phosphatidylserine (PS) lipids.[42-43] Li^{+} also forms strong, high melting dehydrated metal ion-PS complexes and induces bilayer hydrocarbon chain crystallization at higher concentrations.[44-45] Since Co^{2+} is more strongly hydrated than Li^{+}, with hydration enthalpies of 2113 and 545 kJ/mol, respectively,[46] we expect a stronger interaction of Co^{2+} with negatively charged lipid headgroups or an interaction with the headgroup at a lower ion concentration. Yet, we observe compositional asymmetry induced by Co^{2+} at comparable ionic strengths under the conditions of our experiments. A more detailed analysis of the binding thermodynamics and electrostatics, including the determination of the number of cations bound per unit area within the nano-bio interface gap is found in Section F.

F. Quantifying Co^{2+} Adsorption Thermodynamics and Electrostatics in the Nano-Bio-Interface Gap. As shown previously,[47-51] second harmonic generation (SHG) $\chi^{(3)}$ measurements can yield important information about binding thermodynamics and electrostatics.[52-56] SHG spectroscopy adsorption isotherms (Figure 5A) in which the SH signal intensity is monitored as a function of Co^{2+} concentration in the presence of SLBs formed from DMPC and a 9:1 mixture of DMPC and DMPG at a constant salt concentration of 100 mM allow us to explore the role of PG-lipids in promoting Co^{2+} adsorption, to estimate the adsorption Gibbs free energy and the interfacial charge density, and to investigate reversibility, thereby demonstrating the wide utility of the $\chi^{(3)}$ method for studying the nano-bio interface. Figure 5A shows the adsorption of Co^{2+} to single-component lipid bilayers formed solely from DMPC results in little change in the SHG intensity as the Co^{2+} concentration is raised. This finding is similar to the SFG spectroscopy result presented

in Figure 4C, which shows negligible SFG intensity changes upon exposure of bilayers formed from pure DMPC to Co^{2+} ions.

Figure 5A also shows the Co^{2+} adsorption isotherm to bilayers formed from a 9:1 mixture of DMPC and DMPG, revealing that the addition of just 10% of PG-terminated lipid leads to substantial SHG losses as the Co^{2+} concentration is raised. These results are consistent over triplicate measurements on individually formed bilayers of both compositions and consistent with previous studies that indicate divalent cations bind preferentially to anionic phospholipids.[42, 57-59] From the SHG adsorption isotherm and the extracted charge density, it is possible to determine the number of ions present at the interface at the concentration at which we observe the SFG signal intensity increases displayed in Figures 4B and 4D. At 100 mM salt concentration, charge densities are estimated from SHG adsorption isotherms using electrostatic and adsorption models like the combined Gouy-Chapman/Langmuir expression shown in Equation 1.[56]

$$I_{SHG} \propto |E_{SHG}|^2 \propto \left| A + B \sinh^{-1}\left[\left(\sigma_0 + \sigma_{ads}\left\{\frac{K_{ads}[M]}{1+K_{ads}[M]}\right\}\right)\left(\frac{8.44}{\sqrt{M+C_{elec}}}\right)\right]\right|^2 \qquad \text{Eq. 1.}$$

Here, I_{SHG} and E_{SHG} are the second harmonic intensity and second harmonic electric field, respectively, $\sigma_0$is the charge density of the 9:1 DMPC/DMPG bilayer, σ_{ads} is the charge density of the adsorbed Co^{2+} at saturation coverage, K_{ads} is the apparent equilibrium constant of Co^{2+} adsorption in liters per mole, M is the bulk Co^{2+} concentration in moles per liter, and C_{elec} is the background electrolyte concentration (0.1 M NaCl) in moles per liter. As discussed in previously published work, A and B, which contain the second- and third- order nonlinear susceptibilities of the system, and the incident electric field at the fundamental frequency and are treated as constants in our approximations and estimations.[56] The applicability of the Langmuir adsorption model in our case is justified by the observation of near quantitative reversibility in the Co^{2+}/bilayer interaction (Figure 5B).

Fitting Equation 1 to the SHG adsorption data yields a Co^{2+} charge density of 0.1 ± 0.02 C/m^2, corresponding to roughly 3×10^{13} ions/cm^2 at maximum surface coverage if each ion carries a +2 charge. A charge density of 0.1 C/m^2 for Co^{2+} adsorption implies that the surface charge of the SLB is neutralized, as we have previously determined that SLBs formed from 9:1 DMPC/DMPG carry a surface charge density of approximately –0.1 C/m^2.[29, 56] Thus, cobalt ion adsorption to SLBs formed from 9:1 mixtures of DMPC and DMPG appears to result in charge neutralization at the interface. Using the equilibrium constant obtained from the SHG adsorption isotherm shown in Figure 5 (1760 ± 290 M^{-1}), and applying 55.5 M as the standard state for adsorption from solution,[60] ΔG^{Co2+}_{ads} is estimated to be –28 ± 0.4 kJ/mol. This value is comparable to our previous estimates for divalent metal ions binding to mineral oxide surfaces.[54, 61-62] While there are several studies exploring the adsorption behavior of Ca^{2+}, Ni^{2+}, and Mg^{2+} to phospholipids,[57-59, 63] and given the ultra-trace concentrations of cobalt in living systems,[64] little effort has been made to elucidate cobalt adsorption to phospholipid model systems or actual cells in terms of Gibbs free adsorption energies or quantitative surface coverages and electrostatics prior to this present work.

From the Co^{2+} isotherm shown for the SLBs formed from 9:1 DMPC/DMPG (Figure 5A), we estimate that *ca.* 2 x 10^{12} Co^{2+} ions per cm^2 are present at the interface under the conditions for which we observe the SFG signal intensity increases when the bilayer is exposed to 0.5 mg/L, or ~8.5 μM, $CoCl_2$ (Figure 4). Given the comparable SFG signal intensity increases when the bilayer is exposed to this $CoCl_2$ concentration and when it is exposed to 5 mg/L solutions of $LiCoO_2$ nanosheets under otherwise identical buffer and ionic strength conditions, then, we estimate that a *ca.* ten-fold enhancement of Co^{2+} ions in the nano-bio interface gap when compared to the free Co^{2+} ion concentration in 5 mg/L solutions of $LiCoO_2$ nanosheets in 100 mM salt and 10 mM Tris buffer without bilayers present.

As stated above, Figure 5B reveals that cobalt adsorption to supported lipid bilayers formed from 9:1 mixtures of DMPC/DMPG lipids is nearly completely reversible under the conditions explored. In contrast, the SFG experiments we report do not show reversibility, as indicated by the retention in the spectral intensity and lineshapes shown in Figure 4D. These results, taken together, imply that while cobalt ions appear to reversibly adsorb to the bilayer surface, as monitored by SHG spectroscopy, the induced lipid asymmetry upon interaction persists, as revealed by SFG spectroscopy.

IV. CONCLUSIONS. In conclusion, we have investigated the role of electrostatics on the interactions between redox active nanomaterials and supported lipid bilayers. We found that the interactions of $LiCoO_2$ nanosheets with bilayers formed from 9:1 mixtures of DMPC/DMPG depend critically on the ζ-potential of the nanosheets and the ionic strength. By studying metal ion dissolution from $LiCoO_2$ nanosheets, additional information on the mechanism of induced bilayer asymmetry was obtained. Specifically, we found that sub-mg/L concentrations of aqueous metal ions (Li^+ and Co^{2+}) found in bulk $LiCoO_2$ solution do not change the bilayer structure. However, elevated concentrations of aqueous metal ions in the 1 mg/L concentration regime were found to produce SFG signal intensity changes commensurate with induction of compositional asymmetry in the supported lipid bilayers studied here. This outcome is consistent with the notion that the induction of the bilayer asymmetry by $LiCoO_2$ nanosheets occurs through a non-contact mechanism that involves primarily the interaction of negatively charged lipids with dissolved ions concentrated within the electrical double layers present at the nanosheet/bilayer gap. Surface coverage estimates of the Co^{2+} ions within this nano-bio interface gap were obtained by SHG spectroscopy and found to correspond to *ca.* 2×10^{12} Co^{2+} ions per cm^2 for the conditions of nanosheet concentrations that induce membrane asymmetry. SHG and SFG spectroscopy together indicate the observed effects to be specific to the negatively charged DMPG lipids, as

bilayers formed purely from zwitterionic DMPC lipids show none of the effects described for the bilayers that contain DMPG. The observation that just 10% of DMPG lipids lead to the effects described here indicates the ion-lipid interactions are of considerable strength, which is the subject of ongoing work. Whether other lipid types have similar specific interactions with transition metal ions like Co^{2+} is the subject of ongoing work.

Our findings provide opportunities for mitigating non-contact interactions between natural and engineered nanomaterials and biological interfaces. Computational studies aimed at elucidating the thermodynamics of phosphate passivation of $LiCoO_2$ indicate that such an approach is in principle feasible.[21] We therefore suggest that reducing ion dissolution from lithium intercalation compounds, such as the one studied in this work, by intentional surface modifications may provide a path forward for enabling the design of new energy storage materials with reduced environmental impacts through controlled release mechanisms.

ACKNOWLEDGEMENTS. This study was supported by the US National Science Foundation Centers for Chemical Innovation Program, the Center for Sustainable Nanotechnology, under Grant No. CHE-1503408. This work made use of the EPIC and Keck-II facilities of Northwestern University's NU*ANCE* Center, which has received support from the Soft and Hybrid Nanotechnology Experimental (SHyNE) Resource (NSF NNCI-1542205); the MRSEC program (NSF DMR-1121262) at the Materials Research Center; the International Institute for Nanotechnology (IIN); the Keck Foundation; and the State of Illinois, through the IIN. MNH and ACM gratefully acknowledge support of the Graduate Research Fellowship Program of the US National Science Foundation. FMF gratefully acknowledges support through the Friedrich Wilhelm Bessel Prize of the Alexander von Humboldt Foundation.

Supporting Information available. Details regarding the experiments, sample preparation and characterization, and negative controls are available in the Supporting Information.

References

1. Armand, M.; Tarascon, J. M., Building Better Batteries. *Nature* **2008**, *451*, 652-657.
2. Manthiram, A.; Murugan, A. V.; Sarkar, A.; Muraliganth, T., Nanostructured Electrode Materials for Electrochemical Energy Storage and Conversion. *Energy Environ. Sci.* **2008**, *1*, 621-638.
3. Zhang, Q.; Uchaker, E.; Candelaria, S. L.; Cao, G., Nanomaterials for Energy Conversion and Storage. *Chem. Soc. Rev.* **2013**, *42*, 3127-3171.
4. Andre, D.; Kim, S.-J.; Lamp, P.; Lux, S. F.; Maglia, F.; Paschos, O.; Stiaszny, B., Future Generations of Cathode Materials: An Automotive Industry Perspective. *J. Mater. Chem. A* **2015**, *3*, 6709-6732.
5. Belharouak, I.; Sun, Y. K.; Liu, J.; Amine, K., $Li(Ni_{1/3}Co_{1/3}Mn_{1/3})O_2$ as a Suitable Cathode for High Power Applications. *J. Power Sources* **2003**, *123*, 247-252.
6. Nel, A. E.; Madler, L.; Velegol, D.; Xia, T.; Hoek, E. M. V.; Somasundaran, P.; Klaessig, F.; Castranova, V.; Thompson, M., Understanding Biophysicochemical Interactions at the Nano-Bio Interface. *Nat. Mater.* **2009**, *8*, 543-557.
7. Kang, D. H. P.; Chen, M.; Ogunseitan, O. A., Potential Environmental and Human Health Impacts of Rechargeable Lithium Batteries in Electronic Waste. *Environ. Sci. Technol.* **2013**, *47*, 5495-5503.
8. Murphy, C. J., et al., Biological Responses to Engineered Nanomaterials: Needs for the Next Decade. *ACS Cent. Sci.* **2015**, *1*, 117-123.
9. Heinlaan, M.; Ivask, A.; Blinova, I.; Dubourguier, H.-C.; Kahru, A., Toxicity of Nanosized and Bulk ZnO, CuO and TiO_2 to Bacteria Vibrio Fischeri and Crustaceans Daphnia Magna and Thamnocephalus Platyurus. *Chemosphere* **2008**, *71*, 1308-1316.
10. Khanna, P.; Ong, C.; Bay, B.; Baeg, G., Nanotoxicity: An Interplay of Oxidative Stress, Inflammation and Cell Death. *J. Nanomater.* **2015**, *5*, 1163-1180.
11. Gajewicz, A.; Schaeublin, N.; Rasulev, B.; Hussain, S.; Leszczynska, D.; Puzyn, T.; Leszczynski, J., Towards Understanding Mechanisms Governing Cytotoxicity of Metal Oxides Nanoparticles: Hints from Nano-Qsar Studies. *Nanotoxicology* **2015**, *9*, 313-325.
12. Jeng, H. A.; Swanson, J., Toxicity of Metal Oxide Nanoparticles in Mammalian Cells. *J Environ. Sci. Health A Tox. Hazard. Subst. Environ. Eng.* **2006**, *41*, 2699-711.
13. He, X.; Aker, W. G.; Fu, P. P.; Hwang, H.-M., Toxicity of Engineered Metal Oxide Nanomaterials Mediated by Nano-Bio-Eco-Interactions: A Review and Perspective. *Environ. Sci. Nano* **2015**, *2*, 564-582.
14. Puzyn, T.; Rasulev, B.; Gajewicz, A.; Hu, X.; Dasari, T. P.; Michalkova, A.; Hwang, H.-M.; Toropov, A.; Leszczynska, D.; Leszczynski, J., Using Nano-Qsar to Predict the Cytotoxicity of Metal Oxide Nanoparticles. *Nat. Nanotechnol.* **2011**, *6*, 175-178.
15. Fu, P. P.; Xia, Q.; Hwang, H.-M.; Ray, P. C.; Yu, H., Mechanisms of Nanotoxicity: Generation of Reactive Oxygen Species. *J. Food Drug Anal.* **2014**, *22*, 64-75.
16. Hang, M. N.; Gunsolus, I. L.; Wayland, H.; Melby, E. S.; Mensch, A. C.; Hurley, K. R.; Pedersen, J. A.; Haynes, C. L.; Hamers, R. J., Impact of Nanoscale Lithium Nickel Manganese Cobalt Oxide (NMC) on the Bacterium Shewanella Oneidensis Mr-1. *Chem. Mater.* **2016**, *28*, 1092-1100.
17. Gunsolus, I. L.; Hang, M. N.; Hudson-Smith, N. V.; Buchman, J. T.; Bennett, J. W.; Conroy, D.; Mason, S. E.; Hamers, R. J.; Haynes, C. L., Influence of Nickel Manganese Cobalt Oxide Nanoparticle Composition on Toxicity toward Shewanella Oneidensis Mr-1: Redesigning for Reduced Biological Impact. *Environ. Sci. Nano* **2017**, *4*, 636-646.
18. Doğangün, M.; Hang, M. N.; Troiano, J. M.; McGeachy, A. C.; Melby, E. S.; Pedersen, J. A.; Hamers, R. J.; Geiger, F. M., Alteration of Membrane Compositional Asymmetry by $LiCoO_2$ Nanosheets. *ACS Nano* **2015**, *9*, 8755-8765.

19. Xia, T.; Kovochich, M.; Liong, M.; Mädler, L.; Gilbert, B.; Shi, H.; Yeh, J. I.; Zink, J. I.; Nel, A. E., Comparison of the Mechanism of Toxicity of Zinc Oxide and Cerium Oxide Nanoparticles Based on Dissolution and Oxidative Stress Properties. *ACS Nano* **2008**, *2*, 2121-2134.
20. Franklin, N. M.; Rogers, N. J.; Apte, S. C.; Batley, G. E.; Gadd, G. E.; Casey, P. S., Comparative Toxicity of Nanoparticulate ZnO, Bulk ZnO, and $ZnCl_2$ to a Freshwater Microalga (Pseudokirchneriella Subcapitata): The Importance of Particle Solubility. *Environ. Sci. Technol.* **2007**, *41*, 8484-8490.
21. Huang, X.; Bennett, J. W.; Hang, M. N.; Laudadio, E. D.; Hamers, R. J.; Mason, S. E., Ab Initio Atomistic Thermodynamics Study of the (001) Surface of $LiCoO_2$ in a Water Environment and Implications for Reactivity under Ambient Conditions. *J. Phys. Chem. C* **2017,** *121*, 5069-5080.
22. Anglin, T. C.; Conboy, J. C., Kinetics and Thermodynamics of Flip-Flop in Binary Phospholipid Membranes Measured by Sum-Frequency Vibrational Spectroscopy. *Biochemistry US* **2009**, *48*, 10220-10234.
23. Brown, K. L.; Conboy, J. C., Electrostatic Induction of Lipid Asymmetry. *J. Am. Chem. Soc.* **2011**, *133*, 8794-8797.
24. Anglin, T. C.; Liu, J.; Conboy, J. C., Facile Lipid Flip-Flop in a Phospholipid Bilayer Induced by Gramicidin a Measured by Sum-Frequency Vibrational Spectroscopy. *Biophys. J.* **2007**, *92*, L01-L03.
25. Wu, F.-G.; Yang, P.; Zhang, C.; Han, X.; Song, M.; Chen, Z., Investigation of Drug–Model Cell Membrane Interactions Using Sum Frequency Generation Vibrational Spectroscopy: A Case Study of Chlorpromazine. *J. Phys. Chem. C* **2014**, *118*, 17538-17548.
26. Casper, C. B.; Verreault, D.; Adams, E. M.; Hua, W.; Allen, H. C., Surface Potential of DPPC Monolayers on Concentrated Aqueous Salt Solutions. *J. Phys. Chem. B* **2016**, *120*, 2043-2052.
27. Casillas-Ituarte, N. N.; Chen, X. K.; Castada, H.; Allen, H. C., Na^+ and Ca^{2+} Effect on the Hydration and Orientation of the Phosphate Group of DPPC at Air-Water and Air-Hydrated Silica Interfaces. *J. Phys. Chem. B* **2010**, *114*, 9485-9495.
28. Castellana, E. T., Solid Supported Lipid Bilayers: From Biophysical Studies to Sensor Design. *Surf. Sci. Rep.* **2006**, *61*, 429-444.
29. Troiano, J. M.; Olenick, L. L.; Kuech, T. R.; Melby, E. S.; Hu, D.; Lohse, S. E.; Mensch, A. C.; Dogangun, M.; Vartanian, A. M.; Torelli, M. D.;, Ehimiaghe, E.; Walter, A. R.; Fu, L.; Anderton, A. R.; Zhu, Z.; Wang, H.-f.; Orr, G.; Murphy, C. J.; Hamers, R. J.; Pedersen, J. A.; Geiger, F. M. Direct Probes of 4 Nm Diameter Gold Nanoparticles Interacting with Supported Lipid Bilayers. *J. Phys. Chem. C* **2014**, *119*, 534-546.
30. Smoluchowski, M. V. *Phys. Z.* **1905**, *6*, 529-531.
31. Geiger, F. M. Second Harmonic Generation, Sum Frequency Generation, and Chi((3)): Dissecting Environmental Interfaces with a Nonlinear Optical Swiss Army Knife. *Annu. Rev. Phys. Chem.* **2009**, *60*, 61-83.
32. Buchbinder, A. M.; Ray, N. A.; Lu, J.; Van Duyne, R. P.; Stair, P. C.; Weitz, E.; Geiger, F. M., Displacement of Hexanol by the Hexanoic Acid Overoxidation Product at Supported Palladium Nanoparticles under Cyclohexane Solution. *J. Am. Chem. Soc.* **2011**, *133*, 17816-17823.
33. Buchbinder, A. M.; Weitz, E.; Geiger, F. M., When the Solute Becomes the Solvent: Orientation, Ordering, and Structure of Binary Mixtures of 1-Hexanol and Cyclohexane over the (0001) a-Al_2O_3 Surface. *J. Am. Chem. Soc.* **2010**, *132*, 14661-14668.
34. Liu, J.; Conboy, J. C., 1,2-Diacyl-Phosphatidylcholine Flip-Flop Measured Directly by Sum-Frequency Vibrational Spectroscopy. *Biophys. J.* **2005**, *89*, 2522-2532.

35. Olenick, L. L. C., H. M.; Fu, L.; Zhang, Y.; McGeachy, A. C.;; Dogangun, M. W., S. R.; Wang, H-f.; Geiger, F. M., Single-Component Supported Lipid Bilayers Probed Using Broadband Nonlinear Optics. Phys. *Chem. Chem. Phys.*, **2018**, Advance Article.
36. Wen, Y. C.; Zha, S.; Liu, X.; Yang, S. S.; Guo, P.; Shi, G. S.; Fang, H. P.; Shen, Y. R.; Tian, C. S., Unveiling Microscopic Structures of Charged Water Interfaces by Surface-Specific Vibrational Spectroscopy. *Phys. Rev. Lett.* **2016**, *116,* 016101.
37. Sajid, M.; Ilyas, M.; Basheer, C.; Tariq, M.; Daud, M.; Baig, N.; Shehzad, F., Impact of Nanoparticles on Human and Environment: Review of Toxicity Factors, Exposures, Control Strategies, and Future Prospects. *Environ. Sci. Pollut. Res.* **2015**, *22*, 4122-4143.
38. Okur, H. I.; Kherb, J.; Cremer, P. S., Cations Bind Only Weakly to Amides in Aqueous Solutions. *J. Am. Chem. Soc.* **2013**, *135*, 5062-5067.
39. Zimmermann, R.; Küttner, D.; Renner, L.; Kaufmann, M.; Werner, C. Fluidity Modulation of Phospholipid Bilayers by Electrolyte Ions: Insights from Fluorescence Microscopy and Microslit Electrokinetic Experiments. *J. Phys. Chem. A* **2012**, *116*, 6519-6525.
40. Collins, K. D.; Neilson, G. W.; Enderby, J. E. Ions in Water: Characterizing the Forces That Control Chemical Processes and Biological Structure. *Biophys. Chem.* **2007**, *128*, 95-104.
41. Binder, H.; Zschornig, O. The Effect of Metal Cations on the Phase Behavior and Hydration Characteristics of Phospholipid Membranes. *Chem. Phys. Lipids* **2002**, *115*, 39-61.
42. Lau, A.; McLaughlin, A.; McLaughlin, S. The Adsorption of Divalent Cations to Phosphatidylglycerol Bilayer Membranes. *Biochim. Biophys. Acta* **1981**, *645*, 279-92.
43. McLaughlin, A. C. The Interaction of Cobalt with Glycerophosphoryl Glycerol and Phosphatidyl Glycerol Bilayer Membranes. *J. Magn. Reson.* **1982**, *49*, 246-256.
44. Hauser, H.; Shipley, G. G. Interactions of Divalent Cations with Phosphatidylserine Bilayer Membranes. *Biochemistry US* **1984**, *23*, 34-41.
45. López Cascales, J. J.; Garcia de la Torre, J. Effect of Lithium and Sodium Ions on a Charged Membrane of Dipalmitoylphosphatidylserine: A Study by Molecular Dynamics Simulation. *BBA Biomemb.* **1997**, *1330*, 145-156.
46. *Royal Society of Chemistry Data Book: Hydration Enthalpies of Selected Ions*; RSC, 2006.
47. Chen, E. H.; Hayes, P. L.; Nguyen, S. T.; Geiger, F. M., Zinc Interactions with Glucosamine-Functionalized Fused Silica/Water Interfaces. *J. Phys. Chem. C* **2010**, *114*, 19483-19488.
48. Hayes, P. L.; Malin, J. N.; Jordan, D. S.; Geiger, F. M. Get Charged Up: Nonlinear Optical Voltammetry for Quantifying the Thermodynamics and Electrostatics of Metal Cations at Aqueous/Oxide Interfaces. *Chem. Phys. Lett.* **2010**, *499*, 183-192.
49. Ohno, P. E.; Saslow, S. A.; Wang, H.-f.; Geiger, F. M.; Eisenthal, K. B. Phase-Referenced Nonlinear Spectroscopy of the A-Quartz/Water Interface. *Nat. Comm.* **2016**, *7*, 13587.
50. Ohno, P. E.; Wang, H. F.; Geiger, F. M., Second-Order Spectral Lineshapes from Charged Interfaces. *Nat. Comm.* **2017**, *8,* 1032.
51. Ong, S. W.; Zhao, X. L.; Eisenthal, K. B., Polarization of Water-Molecules at a Charged Interface - 2nd Harmonic Studies of the Silica Water Interface. *Chem. Phys. Lett.* **1992**, *191*, 327-335.
52. Achtyl, J. L.; Vlassiouk, I. V.; Surwade, S. P.; Fulvio, P. F.; Dai, S.; Geiger, F. M., Interaction of Magnesium Ions with Pristine Single-Layer and Defected Graphene/Water Interfaces Studied by Second Harmonic Generation. *J. Phys. Chem. B* **2014**, *118*, 7739-7749.

53. Malin, J. N.; Geiger, F. M., Uranyl Adsorption and Speciation at the Fused Silica/Water Interface Studied by Resonantly Enhanced Second Harmonic Generation and the Chi((3)) Method. *J. Phys. Chem. A* **2010**, *114*, 1797-1805.
54. Malin, J. N.; Hayes, P. L.; Geiger, F. M., Interactions of Ca, Zn, and Cd Ions at Buried Solid/Water Interfaces Studied by Second Harmonic Generation. *J. Phys. Chem. C* **2009**, *113*, 2041-2052.
55. Troiano, J. M.; Kuech, T. R.; Vartanian, A. M.; Torelli, M. D.; Sen, A.; Jacob, L. M.; Hamers, R. J.; Murphy, C. J.; Pedersen, J. A.; Geiger, F. M. On Electronic and Charge Interference in Second Harmonic Generation Responses from Gold Metal Nanoparticles at Supported Lipid Bilayers. *J. Phys. Chem. C* **2016**, *120*, 20659-20667.
56. Troiano, J. M., McGeachy, A. C.; Olenick, L. L.; Fang, D.; Liang, D.; Hong, J.; Kuech, T. R.; Caudill, E. R.; Pedersen, J. A.; Cui, Q.; Geiger, F. M. Quantifying the Electrostatics of Polycation-Lipid Bilayer Interactions. *J. Am. Chem. Soc.* **2017**, *139*, 5808-5816.
57. Javanainen, M.; Melcrova, A.; Magarkar, A.; Jurkiewicz, P.; Hof, M.; Jungwirth, P.; Martinez-Seara, H., Two Cations, Two Mechanisms: Interactions of Sodium and Calcium with Zwitterionic Lipid Membranes. *Chem. Commun.* **2017**, *53*, 5380-5383.
58. Lehrmann, R.; Seelig, J., Adsorption of Ca2+ and La3+ to Bilayer-Membranes - Measurement of the Adsorption Enthalpy and Binding Constant with Titration Calorimetry. *BBA - Biomemb.* **1994**, *1189*, 89-95.
59. Melcrova, A.; Pokorna, S.; Pullanchery, S.; Kohagen, M.; Jurkiewicz, P.; Hof, M.; Jungwirth, P.; Cremer, P. S.; Cwiklik, L., The Complex Nature of Calcium Cation Interactions with Phospholipid Bilayers. *Sci. Rep.* **2016**, *6*, 38035.
60. Adamson, A. W., *Physical Chemistry of Surfaces*, 5th ed.; John Wiley & Sons: New York, 1990.
61. Chen, E. H.; Saslow, S. A.; Nguyen, S. T.; Geiger, F. M., Zinc Ion-Hydroxyl Interactions at Undecanol-Functionalized Fused Silica/Water Interfaces Using the Eisenthal Chi((3)) Technique. *J. Phys. Chem. C* **2012**, *116*, 7016-7020.
62. Hayes, P. L.; Malin, J. N.; Konek, C. T.; Geiger, F. M., Interaction of Nitrate, Barium, Strontium and Cadmium Ions with Fused Quartz/Water Interfaces Studied by Second Harmonic Generation. *J. Phys. Chem. A* **2008**, *112*, 660-668.
63. Mclaughlin, A.; Grathwohl, C.; Mclaughlin, S., Adsorption of Divalent-Cations to Phosphatidylcholine Bilayer Membranes. *Biochim. Biophys. Acta* **1978**, *513*, 338-357.
64. Okamoto, S.; Eltis, L. D., The Biological Occurrence and Trafficking of Cobalt. *Metallomics* **2011**, *3*, 963-970.

Table I. Apparent ζ-Potentials[a] for Fresh Suspensions (5mg/L) of $LiCoO_2$ Nanosheets in 0.001 M or 0.1 M NaCl and 0.01 M HEPES or Tris Buffer at pH 7.4 and Corresponding Observed Changes in SFG Signal Intensity Upon Exposure of SLBs Made from 9:1 Mixtures of DMPC/DMPG Lipids.

[NaCl] (M)	Buffering agent (0.01M)	Apparent ζ-Potential (mV)	ΔI_{SFG}
0.1	Tris	+12.9 ± 0.6	Increase by +2.0±0.7
0.1	HEPES	-19.4 ± 1.8	No change
0.001	Tris	-9.4 ± 0.8	No change
0.001	HEPES	-20.5 ± 0.3	Not measured

[a]Estimate assumes spherical particles.

Table II. Measured Concentrations of Ions Produced by Dissolution in a 5 mg/L Solution of $LiCoO_2$ Nanosheets.[a]

Buffer	Dissolved metal ion concentration (mg/L)			
	Li (mg/L)	Li (μM)	Co (mg/L)	Co (μM)
0.1 M NaCl, 0.01M Tris	0.124 ± 0.002	17.86 ± 0.29	0.042 ± 0.001	0.71 ± 0.01
0.001 M NaCl, 0.01M Tris	0.206 ± 0.001	29.68 ± 0.20	0.029 ± 0.001	0.49 ± 0.05
0.1 M NaCl, 0.01M HEPES	0.283 ± 0.004	40.77 ± 0.61	0.035 ± 0.004	0.59 ± 0.07

[a] The mean and standard deviation of three replicate samples are listed for the measured values.

Figure Captions

Figure 1: SEM images and EDS spectra from numbered areas indicated of bilayers formed from a 9:1 mixture of DMPC/DMPG in (A) 0.01 M Tris buffer, 0.1 M NaCl at 23°C and pH 7.4 upon exposure to $LiCoO_2$ nanosheets (5 mg/L) and rinsing, and (B) 0.01 M HEPES buffer, 0.1 M NaCl at 23°C and pH 7.4 upon exposure to $LiCoO_2$ nanosheets (5 mg/L) and rinsing.

Figure 2: *ssp*-Polarized SFG spectra of bilayers formed from 9:1 mixture of DMPC/DMPG lipids at 22 °C and pH 7.4 in (A) 0.1 M NaCl, 0.01M Tris buffer before (green) and after (black) exposure to $LiCoO_2$ nanosheets (5 mg/L) (B) 0.1 M NaCl, 0.01M HEPES buffer before (green) and after (black) exposure to $LiCoO_2$ nanosheets (5 mg/L) (C) 0.1 M NaCl, 0.01 M Tris buffer (green), 0.01 M NaCl, 0.01M Tris buffer (blue) (D) 0.01 M NaCl, 0.01 M Tris buffer before (blue) and after (black) exposure to $LiCoO_2$ nanosheets (5 mg/L).

Figure 3: *ssp*-Polarized SFG spectra of bilayers formed from 9:1 mixture of DMPC/DMPG lipids before (green) and after exposure to (A) 0.1 mg/L Li^+ (black), (B) 0.05 mg/L Co^{2+} (purple), (C) a mixture of 0.1 mg/L Li^+ and 0.05 mg/L Co^{2+} (black), and (D) 1 mg/L NaCl (dark green), all in 0.01 M Tris buffer, 0.1 M NaCl, and at 22 °C and pH 7.4.

Figure 4: *ssp*-Polarized SFG spectra of bilayers formed from 9:1 mixture of DMPC/DMPG lipids before (green) and after exposure to (A) 1 mg/L Li^+ (black), (B) 0.5 mg/L Co^{2+} (purple). (C) *ssp*-Polarized SFG spectra of bilayer formed from 100% DMPC lipids before (green) and after exposure to 1 mg/L Li^+ (black). (D) *ssp*-Polarized SFG spectra of bilayers formed from 9:1 mixture of DMPC/DMPG lipids before (green) and after exposure to 0.5 mg

Co^{2+} and rinsing. All data recorded in 0.01 M Tris buffer, 0.1 M NaCl, and at 22 °C and pH 7.4.

Figure 5: (**A**) Normalized SHG E-field as a function of bulk cobalt chloride concentration in the presence of supported lipid bilayers formed from DMPC (open circles) and 9:1 mixtures of DMPC and DMPG (filled circles) at 0.1 M NaCl (0.01 M Tris buffer, pH 7.4), and fit of the combined Gouy-Chapman and Langmuir model (solid black line). (**B**) Time trace of the normalized SHG E-field (left-axis) with a sliding average of 10 seconds (gray) and 50 seconds (black) and incident laser power (dots, right-axis) before and during the exposure of a SLB formed from a 9:1 mixture of DMPC and DMPG at 0.1 M NaCl (0.01 M Tris buffer, pH 7.4) to 0.001 M cobalt chloride at t=53 min, followed by rinsing in cobalt-free buffer at t=80 min.

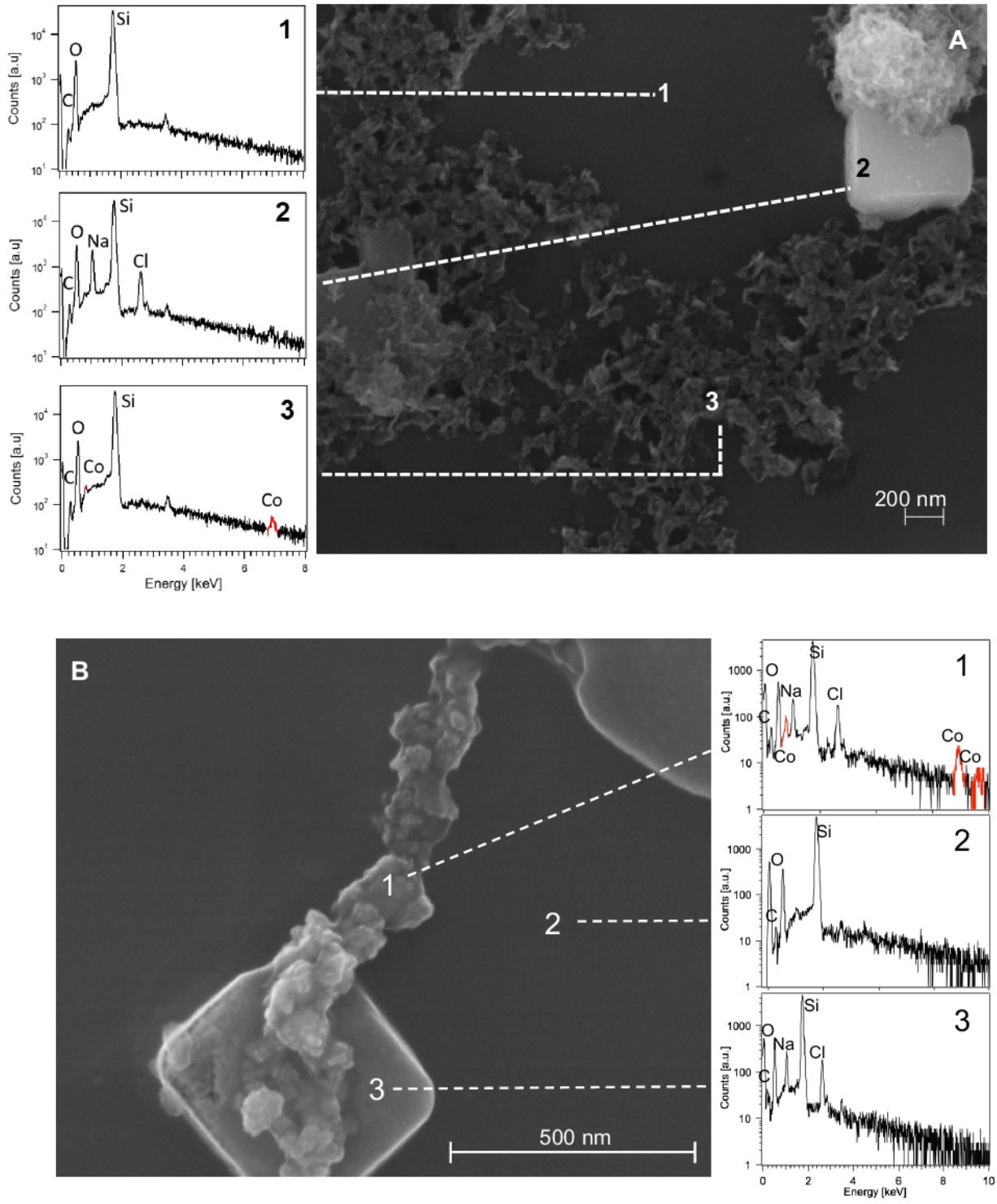

Figure 1

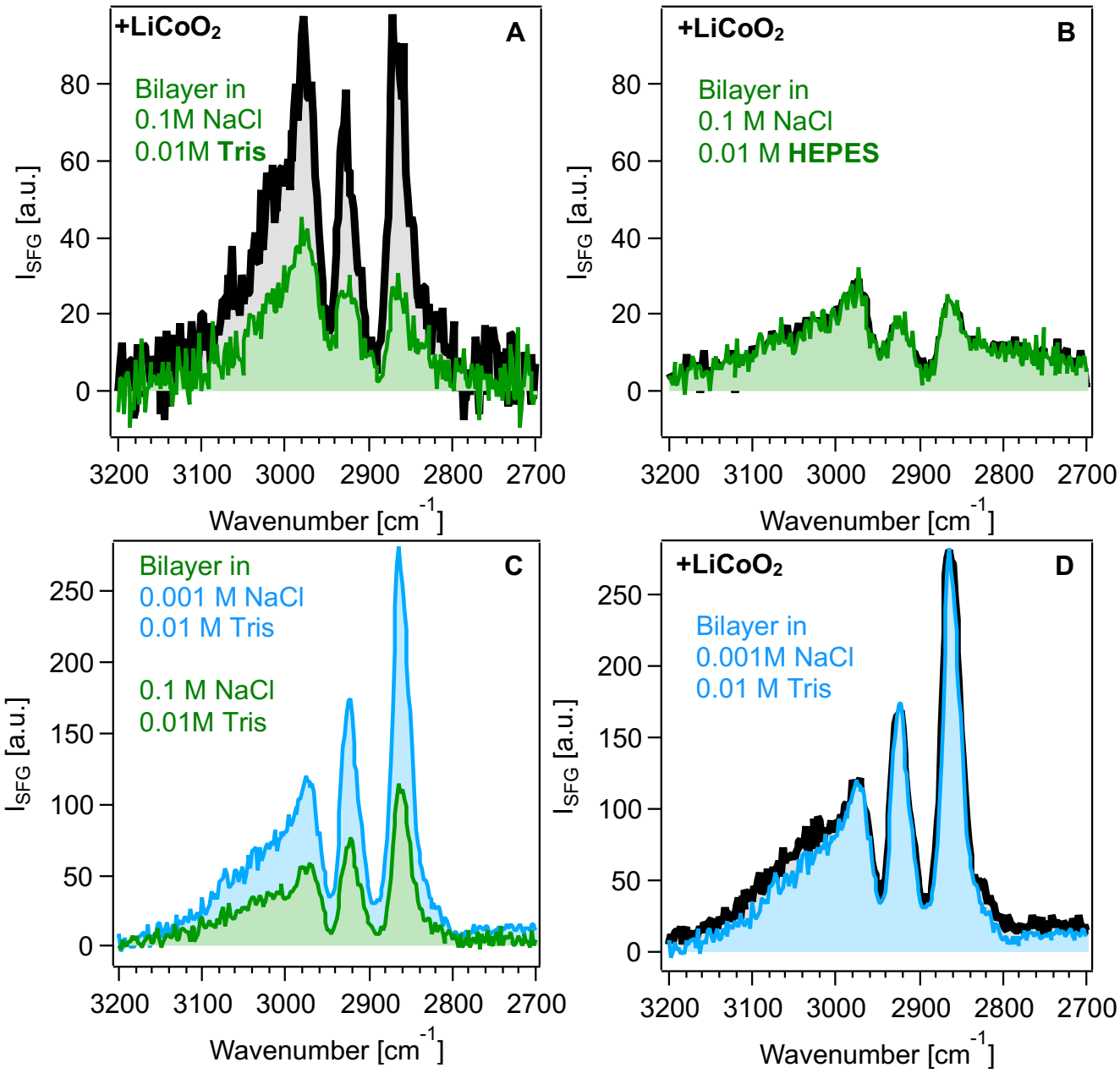
+LiCoO2
A
Bilayer in
0.1M NaCl
0.01M Tris
ISFG [a.u.]
Wavenumber [cm-1]
+LiCoO2
B
Bilayer in
0.1 M NaCl
0.01 M HEPES
ISFG [a.u.]
Wavenumber [cm-1]
C
Bilayer in
0.001 M NaCl
0.01 M Tris
0.1 M NaCl
0.01M Tris
ISFG [a.u.]
Wavenumber [cm-1]
+LiCoO2
D
Bilayer in
0.001M NaCl
0.01 M Tris
ISFG [a.u.]
Wavenumber [cm-1]

Figure 2

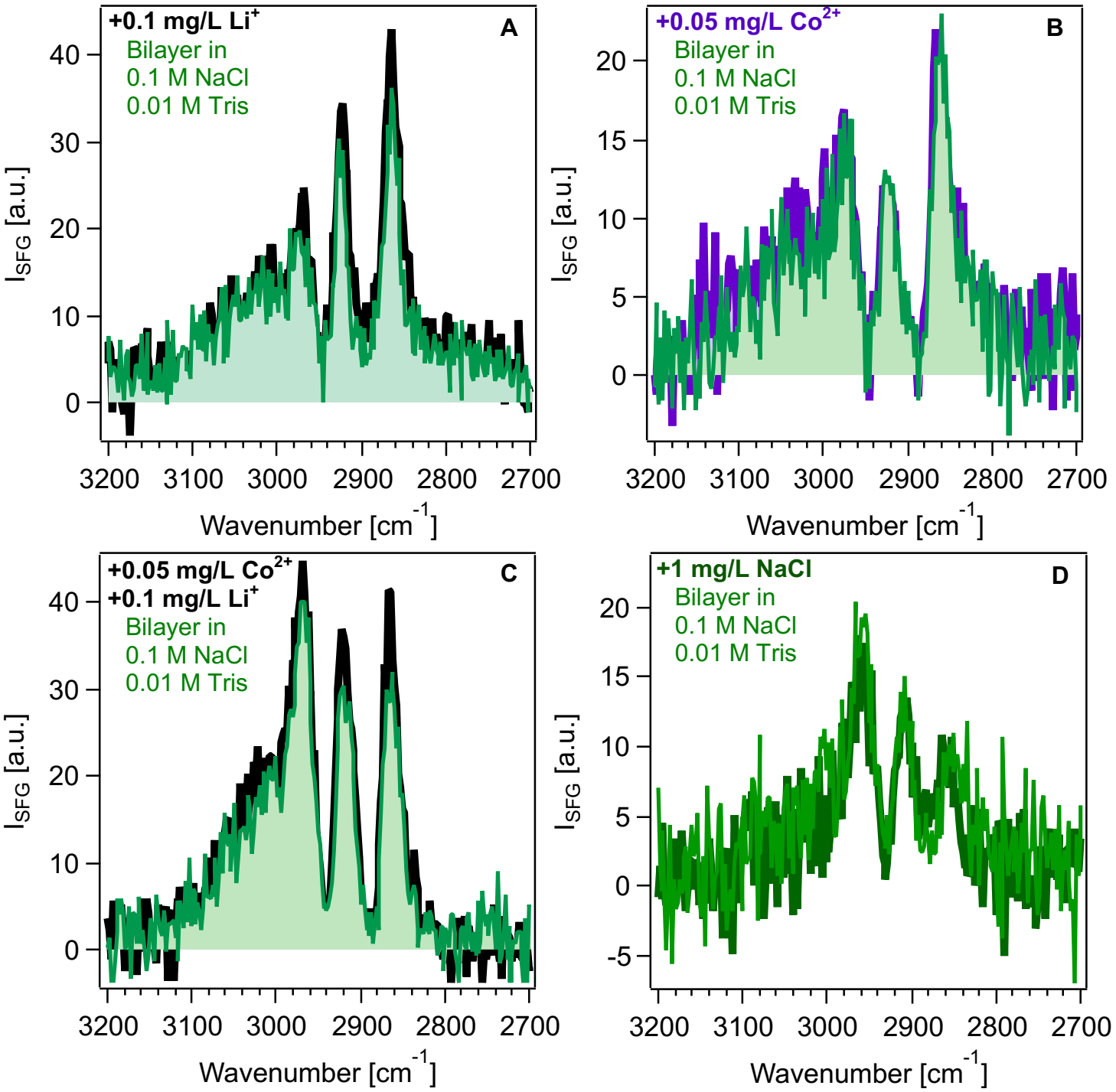
+0.1 mg/L Li+
Bilayer in
0.1 M NaCl
0.01 M Tris
A
+0.05 mg/L Co2+
Bilayer in
0.1 M NaCl
0.01 M Tris
B
+0.05 mg/L Co2+
+0.1 mg/L Li+
Bilayer in
0.1 M NaCl
0.01 M Tris
C
+1 mg/L NaCl
Bilayer in
0.1 M NaCl
0.01 M Tris
D
ISFG [a.u.]
Wavenumber [cm-1]
3200 3100 3000 2900 2800 2700

Figure 3

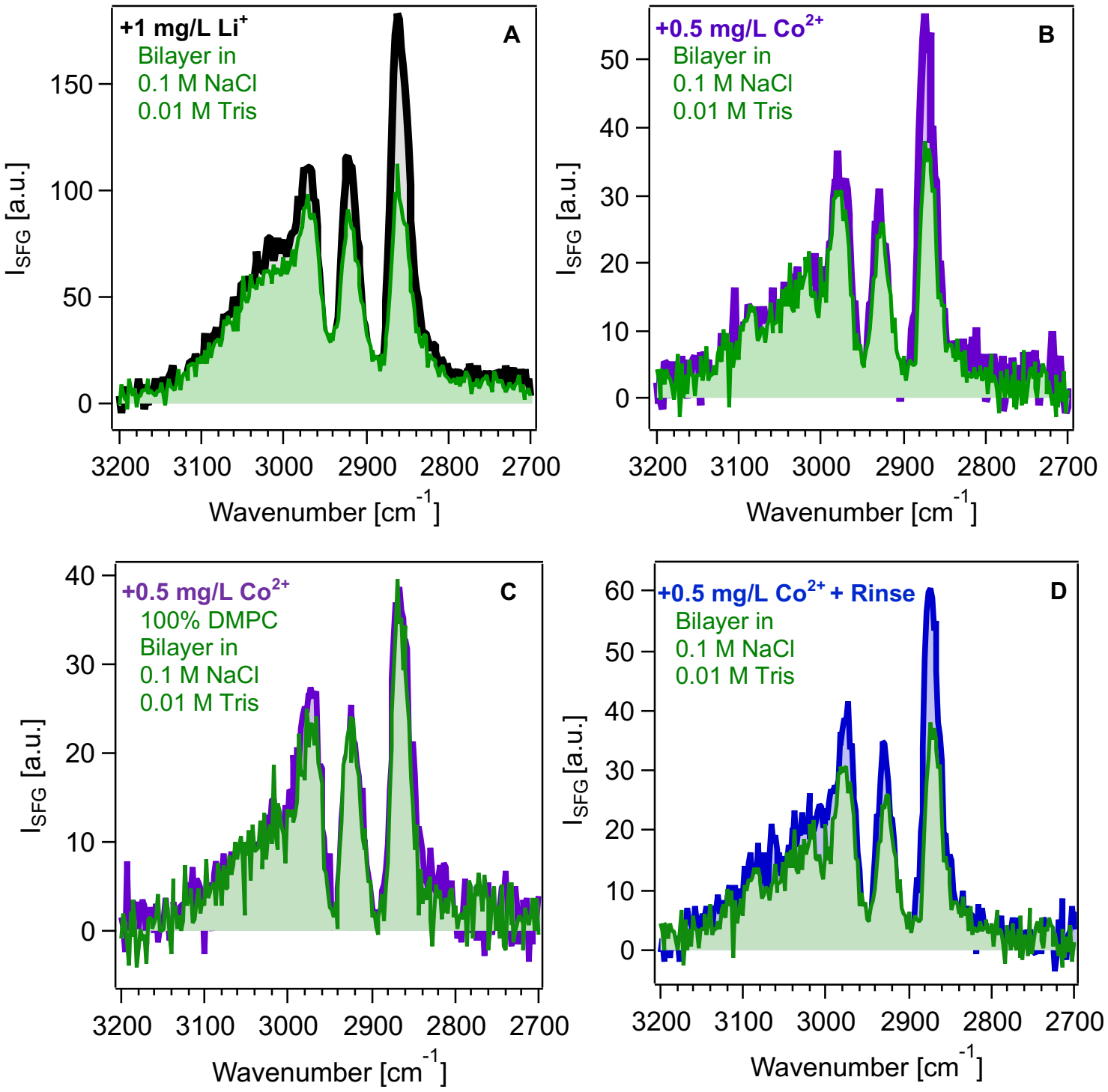
+1 mg/L Li+
Bilayer in
0.1 M NaCl
0.01 M Tris
A
+0.5 mg/L Co2+
Bilayer in
0.1 M NaCl
0.01 M Tris
B
+0.5 mg/L Co2+
100% DMPC
Bilayer in
0.1 M NaCl
0.01 M Tris
C
+0.5 mg/L Co2+ + Rinse
Bilayer in
0.1 M NaCl
0.01 M Tris
D
ISFG [a.u.]
Wavenumber [cm-1]

Figure 4

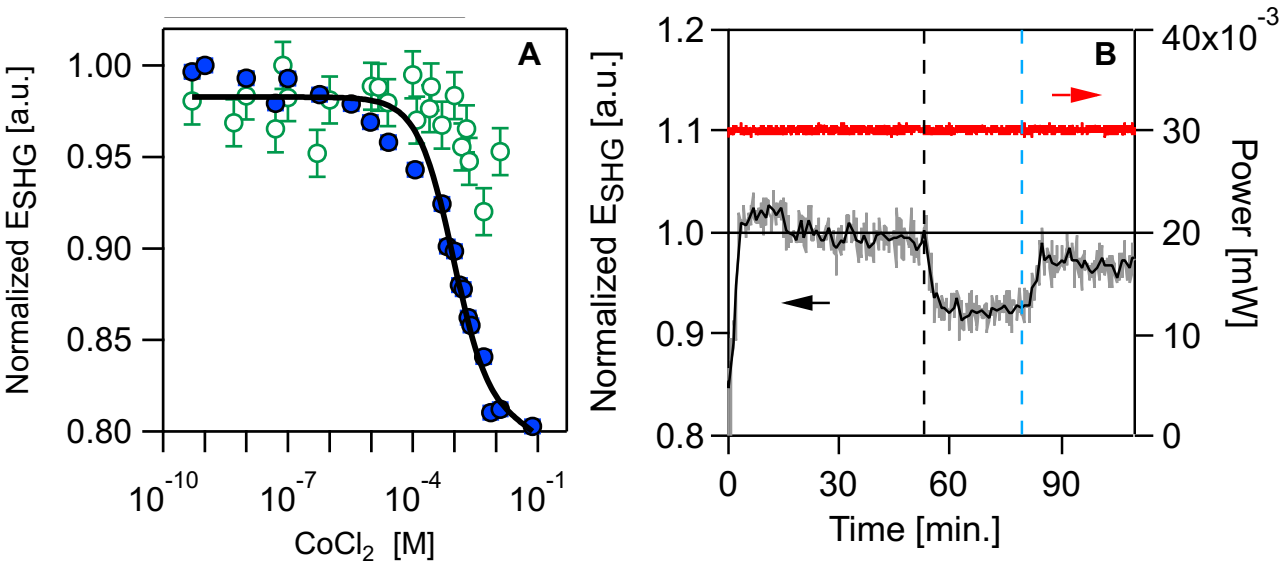
A
Normalized E_{SHG} [a.u.]
1.00
0.95
0.90
0.85
0.80
10^{-10}
10^{-7}
10^{-4}
10^{-1}
$CoCl_2$ [M]
B
Normalized E_{SHG} [a.u.]
1.2
1.1
1.0
0.9
0.8
40x10^{-3}
30
20
10
0
Power [mW]
0
30
60
90
Time [min.]

Figure 5

TOC Graphic